Collision-Induced Dissociation Measurements on $Li^+(H_2O)_n$, $n = 1-6$: The First Direct Measurement of the Li^+-OH_2 Bond Energy

M. T. Rodgers and P. B. Armentrout*

Department of Chemistry, University of Utah, Salt Lake City, Utah 84112

Received: July 17, 1996; In Final Form: October 3, 1996[⊗]

Collision-induced dissociation of $Li^+(H_2O)_n$, $n = 1-6$, with xenon (and with argon for $n = 1$) is studied as a function of kinetic energy using guided ion beam mass spectrometry. In all cases, the primary and lowest energy dissociation channel observed is endothermic loss of one water molecule. The cross section thresholds are interpreted to yield 0 and 298 K bond energies after accounting for the effects of multiple ion−molecule collisions, internal energy of the complexes, and dissociation lifetimes. The experimental bond energies determined here are in good agreement with previous experimental (high-pressure mass spectrometric, HPMS, measurements) and theoretical results for all complexes. In the case of $Li^+(H_2O)$, the value determined here is actually the first direct measurement of the bond energy. This value lies somewhat below the value reported in the HPMS study which was extrapolated from data for larger clusters. Because the HPMS value has been used extensively to establish an absolute Li^+ affinity scale, this discrepancy is discussed in some detail.

Introduction

The functionality of biological molecules is strongly influenced by their three-dimensional structures, which are primarily determined through noncovalent interactions with metal ions, hydrogen-bonding interactions, and solvation. One means of obtaining a more detailed understanding of such effects is through quantitative studies in the gas phase where individual interactions can be examined. In the present study, we examine a simple metal−solvent system, $Li^+(H_2O)_n$, $n = 1-6$, clusters. This system acts as a fundamental model for solvation effects and also incorporates noncovalent metal−ligand interactions and hydrogen bonding (for $n = 5$ and 6).

Although the $Li^+(H_2O)_n$ clusters are intrinsically interesting, the detailed study presented here came about as a result of ongoing studies designed to measure the binding energies of biologically relevant metal ion−ligand interactions. Our approach is to use guided ion beam mass spectrometry to examine the kinetic energy dependence of collision-induced dissociation (CID) reactions of $M^+(L)_n$ complexes. Experimental difficulties in such measurements arise from internal energy randomization that can increase the lifetime of the energized molecule until it exceeds the experimental time window available. This results in a kinetic shift, a reduced sensitivity for measuring the true thermodynamic onset for the CID process, that becomes more noticeable as the size of the molecule increases. We have previously described a means of estimating this effect by incorporating RRKM theory,[1] which predicts the unimolecular rate of dissociation of an energized molecule, in our data analysis. Such lifetime effects should be particularly important for the large biomolecules we are studying. Clearly, the reliability of CID threshold measurements in these systems will be enhanced if the assumptions needed to include the rate of unimolecular decomposition can be put on a firmer theoretical basis and empirically confirmed. We have recently revised our method of estimating parameters needed for this RRKM analysis and detail this procedure elsewhere.[2,3] In that work, we study the Li^+ binding affinities of various short-chain alcohols, a good test case because previous equilibrium measurements[4] are available for comparison. However, this comparison is complicated by incorrect adjustments for differing experimental temperatures and by the fact that the absolute Li^+ affinities reported in the equilibrium study (and others throughout the literature) can be traced back to the value of $D(Li^+-OH_2)$ reported by Dzidic and Kebarle (DK).[5] This bond energy was not measured directly, but was extrapolated from measurements made for larger $Li^+(H_2O)_n$ clusters. Thus, the present study provides the first direct measurement of the Li^+-OH_2 bond energy. To assess possible systematic differences between the results of the present study and those of DK,[5] we also extend our measurements of $Li^+(H_2O)_n$ binding affinities to include clusters containing up to six water molecules. In addition, the present work provides another test of our revised method of RRKM analysis.

Previous work designed to measure the thermodynamics of $M^+(H_2O)_n$ clusters has included several techniques. Chief among these are equilibrium studies, in either an ion cyclotron resonance (ICR) mass spectrometer or a high-pressure mass spectrometer (HPMS), and energy-resolved CID studies. The binding energies of metal ions of the first transition series to H_2O have been studied using CID methods by Marinelli and Squires,[6] Magnera et al.,[7] Magnera, David, and Michl,[8] Schultz and Armentrout,[9] and Dalleska, Honma, Sunderlin, and Armentrout (DHSA),[10] with generally good agreement achieved. For the case of $Cu^+(H_2O)_n$, $n = 3$ and 4, good agreement between the CID results of DHSA and the HPMS results of Holland and Castleman[11] was found. Likewise, CID studies of $Na^+(H_2O)_n$, $n = 1-4$, by Dalleska, Tjelta, and Armentrout (DTA)[12] yield bond energies in good agreement with the HPMS results of DK.[5] DK also studied the $Li^+(H_2O)_n$, $n = 2-6$, cluster system of immediate interest here. Additional work on Li^+−water interactions includes the ICR equilibrium studies of Woodin and Beauchamp (WB)[13] and of Taft et al.,[4] although these studies include only relative thermodynamic information. Indeed, WB anchored their relative Li^+ binding affinities to the Li^+-OH_2 bond energy estimated by DK and determined a Li^+-NH_3 bond energy relative to this. Taft et al. then anchored their relative Li^+ binding affinities to the Li^+-NH_3 bond energy reported by WB. Since this time, Bojesen et al.[14] and Cerda and Wesdemiotis[15] have used Cooks kinetic method to determine Li^+ affinities of various bases, where again the absolute anchor

[⊗] Abstract published in *Advance ACS Abstracts,* January 15, 1997.

S1089-5639(96)02170-6 CCC: $14.00

TABLE 1: Vibrational Frequencies and Average Vibrational Energies at 298 K[a]

species	E_{vib},[b] eV	frequencies, cm^{-1}
H_2O	0.0001(0.0001)	1622, 3804, 3938
$Li^+(H_2O)$[c]	0.022(0.003)	354, 504, **528**, 1660, 3775, 3874
$Li^+(H_2O)_2$[c]	0.113(0.007)	73(2), 106, **269**, 330(2), 490(2), **661**, 1660, 1661, 3783, 3774, 3887(2)
$Li^+(H_2O)_3$[c]	0.207(0.012)	58(2), 82(2), 94, 182, **251**, 289, 291(2), 416(2), 438, **567**(2), 1652(2), 1654, 3793(2), 3795, 3903, 3904(2)
$Li^+(H_2O)_4$[d]	0.309(0.038)	52, 55(3), 100, 126(2), 129, 207, 216, 260(2), 263, 301, 324(2), 350, **368**, **469**(2), **476**, 1589, 1590(2), 1593, 3700(3), 3703, 3785(4)
$Li^+(H_2O)_5$[d]	0.383(0.049)	23, 56, 67, 68, 89, 103, 121, 122, **158**, 173, 202, 205, 207, 223, 228, 260, 280, 321, 340, 353, 385, 428, 429, 478, 487, 553, 559, 1579, 1583, 1586, 1589, 1606, 3637, 3651, 3695, 3703, 3705, 3775, 3778(2), 3790(2)
$Li^+(H_2O)_6$[d]	0.464(0.060)	30(2), 41, 81(2), 84, 113(2), 120, 138, **161**, **167**, 189, 190, 203, 208, 214(2), 227, 233, 329(2), 382(2), 393, 449(2), 470, 472, 481, 548(2), 562, 1574(2), 1581, 1583, 1604(2), 3649(2), 3659, 3663, 3693(2), 3776(2), 3783(2), 3786(2)

[a] Frequencies taken from ref 23. The reaction coordinate is indicated in boldface (when more than one frequency is in bold, an average of the frequencies was used). [b] Uncertainties in the average vibrational energies listed in parentheses are determined as described in the text. [c] Vibrational frequencies determined at the MP2 level. [d] Vibrational frequencies determined at the RHF level scaled by 0.9.

for the values they measure relies on the extrapolated value for $Li^+(H_2O)$ reported by DK. The lithium water clusters have also been examined theoretically with numerous studies of the $Li^+(H_2O)$ cluster,[16−21] but only two for the larger $Li^+(H_2O)_n$ systems.[22,23]

Experimental Section

General Procedures. Cross sections for CID of lithium ion−water clusters are measured using a guided ion beam mass spectrometer that has been described in detail previously.[24,25] The metal ion bound water clusters are generated as described below. The ions are extracted from the source, accelerated, and focused into a magnetic sector momentum analyzer for mass analysis. Mass-selected ions are decelerated to a desired kinetic energy and focused into an octopole ion guide that traps the ions in the radial direction.[26] The octopole passes through a static gas cell containing xenon, used as the collision gas for reasons described elsewhere,[10,27,28] or argon, used for reasons described below. Pressures of the collision gases, Xe or Ar, in the gas cell are kept low (typically 0.03−0.20 mTorr) to ensure that multiple ion−molecule collisions are improbable. Product and unreacted parent cluster ions drift to the end of the octopole where they are focused into a quadrupole mass filter for mass analysis and subsequently detected with a secondary electron scintillation detector and standard pulse counting techniques.

Ion intensities are converted to absolute cross sections as described previously.[24] Absolute uncertainties in cross section magnitudes are estimated to be ±20%, which is largely the result of uncertainties in the pressure measurement and the length of the interaction region. Relative uncertainties are approximately ±5%. Because the radio frequency used for the octopole does not trap light masses with high efficiency, the cross sections for Li^+ products were more sensitive to focusing conditions and showed more variations in magnitude than is typical for this apparatus. Therefore, the absolute magnitudes of the cross sections for production of Li^+ are probably about ±50%.

Ion kinetic energies in the laboratory frame, E_{Lab}, are converted to energies in the center-of-mass frame, E_{CM}, using the formula $E_{CM} = E_{Lab}m/(m + M)$, where M and m are the masses of the reactant ion and neutral molecules, respectively. All energies reported below are in the CM frame unless otherwise noted. The absolute zero and distribution of the ion kinetic energies are determined using the octopole ion guide as a retarding potential analyzer as previously described.[24] The distribution of ion kinetic energies is nearly Gaussian with a fwhm typically between 0.2 and 0.3 eV (Lab) for these experiments. The uncertainty in the absolute energy scale is ±0.05 eV (Lab).

Even when the pressure of the reactant neutral is low, we have previously demonstrated that the effects of multiple collisions can significantly influence the shape of CID cross sections.[30] Because the presence and magnitude of these pressure effects are difficult to predict, we have performed pressure-dependent studies of all cross sections examined here. Data free from pressure effects can always be obtained by extrapolating to zero pressure, as described previously.[10] In the systems studied here, we found no dependence on Xe or Ar pressure up to the highest pressure examined, ∼0.2 mTorr.

Ion Source. The lithium ion-water clusters are formed in a 1 m long flow tube[25,29] operating at a pressure of 0.5−0.7 Torr with a helium flow rate of 4000−7000 sccm. Metal ions are generated in a continuous dc discharge by argon ion sputtering of a cathode, made from tantalum or iron, with a cavity containing lithium metal. Typical operating conditions of the discharge are 1.5−3 kV and 20−30 mA in a flow of roughly 10% argon in helium. The lithium ion−water clusters are formed by associative reactions of the lithium ion with water molecules that are introduced into the flow 50 cm downstream from the dc discharge. The flow conditions used in this ion source provide in excess of 10^4 collisions between an ion and the buffer gas, which should thermalize the ions both vibrationally and rotationally. In our analysis of the data, we assume that the ions produced in this source are in their ground electronic states and that the internal energy of the lithium ion−water clusters is well-described by a Maxwell−Boltzmann distribution of vibrational and rotational states corresponding to 300 K. Previous work from this laboratory has shown that these assumptions are valid.[1,10,29−33]

Thermochemical Analysis. The threshold regions of the reaction cross sections are modeled using eq 1,

$$\sigma = \sigma_0 \sum_i g_i (E + E_i - E_0)^n / E \qquad (1)$$

where σ_0 is an energy-independent scaling factor, E is the relative translational energy of the reactants, E_0 is the threshold for reaction of the ground electronic and ro-vibrational state, and n is an adjustable parameter. The summation is over the ro-vibrational states of the reactant ions, i, where E_i is the excitation energy of each state and g_i is the population of those states ($\Sigma g_i = 1$). The populations of excited ro-vibrational levels are not negligible even at 300 K as a result of the many low-frequency modes present in these ions. It is assumed that n and σ_0 in eq 1 are the same for all states.

The vibrational frequencies of the $Li^+(H_2O)_n$ clusters used in this work are listed in Table 1. These were obtained from Feller, Glendening, Kendall, and Peterson (FGKP) and are based on their published theoretical work.[23] Because of the difficulty associated with these calculations for large systems, varying levels of theory were used depending upon the size of the water cluster. For $Li^+(H_2O)_n$, $n = 1-3$, the frequencies were

TABLE 2: Rotational Constants of $Li^+(H_2O)_n$ in cm^{-1}

	energized molecule		transition state		
species	1-D[a]	2-D[b]	1-D[a]	2-D[b]	1-D[c]
$Li^+(H_2O)$	14.19	0.84	14.19	0.094	9.28, 27.79
$Li^+(H_2O)_2$	7.10	0.12	7.10	0.028	0.80, 0.85, 9.28, 14.50, 27.79
$Li^+(H_2O)_3$	0.077	0.15	0.12	0.032	0.12, 7.10, 9.28, 14.50, 27.79
$Li^+(H_2O)_4$	0.085	0.082	0.077	0.027	0.15, 0.15, 9.28, 14.50, 27.79
$Li^+(H_2O)_5$	0.093	0.039	0.084	0.023	0.082, 0.085, 9.28, 14.50, 27.79
$Li^+(H_2O)_6$	0.100	0.021	0.100	0.0086	0.040, 0.038, 9.28, 14.50, 27.79

[a] Active external. [b] Inactive external. [c] Rotational constants of transitional modes treated as free internal rotors.

determined from a vibrational analysis of the geometry-optimized structures of the clusters obtained at the MP2 level. Because frequencies determined at the MP2 level generally reproduce the vibrational spectrum quite well, all MP2 vibrational frequencies are used in our analysis without scaling. For $n = 4-6$, the frequencies were determined from a vibrational analysis of the geometry optimized structures of the clusters obtained at the RHF level. Vibrational frequencies calculated at this level of theory tend to be greater than experimentally measured frequencies; however, studies over the past two decades have established that the discrepancy between the computed and experimental force constants is sufficiently systematic to allow the application of generalized scaling procedures which bring the computed vibrational spectrum into agreement with experiment.[34] For frequencies determined at the RHF level, the generalized scaling factor typically used is 0.9, and this factor is used for all RHF vibrational frequencies in our analyses. Rotational constants of all clusters, listed in Table 2, were calculated using the published geometries of the $Li^+(H_2O)_n$ clusters of FGKP.[23] The Beyer−Swinehart[35,36] algorithm is used to calculate the population distribution of rovibrational states using these frequencies and rotational constants.

The geometries of $Li^+(H_2O)_n$, $n = 1-6$, determined by FGKP[23] deserve mention because the vibrational frequencies and rotational constants used in our analysis were derived from these structures. Further, these geometries lead to a better understanding of the trends in the measured BDEs and cross section magnitudes. $Li^+(H_2O)$ has C_{2v} symmetry, such that the in-plane oxygen lone pair points directly at the lithium ion. The lowest energy configuration of $Li^+(H_2O)_2$ is one where the water molecules are bound to opposite sides of the lithium ion and twisted 90° with respect to each other, in a symmetric D_{2d} configuration. The lowest energy conformation of $Li^+(H_2O)_3$ is one in which all three oxygen atoms form a planar equilateral triangle around the lithium ion. The hydrogen atoms are rotated such that the cluster has D_3 symmetry. The lowest energy conformation of $Li^+(H_2O)_4$ has S_4 symmetry, with the oxygen atoms in a tetrahedral arrangement around the lithium ion. For complexes containing up to four water molecules, the lowest energy conformation corresponds to the structure in which every water molecule is bonded directly to the central lithium ion. For $Li^+(H_2O)_5$, a stable structure having all five water molecules directly coordinated to the lithium ion was calculated, but the most stable structure (having C_2 symmetry) calculated has the fifth water molecule bound through two hydrogen bonds to two of the four water molecules in the first solvent shell. Similarly, the lowest energy configuration of $Li^+(H_2O)_6$ has C_2 symmetry with the fifth and sixth water molecules each bound through two hydrogen bonds to opposite pairs of the four water molecules in the first solvent shell.

Another consideration in the analysis of CID thresholds is whether dissociation occurs within the time scale of the experiment, approximately 10^{-4} s in our instrument. If the lifetime of the collisionally excited ion exceeds this, then a kinetic shift will be observed as an increase in the apparent threshold. This effect is included in our threshold analysis by incorporation of RRKM theory in eq 1, as has been described in detail previously.[1−3,37] Briefly, eq 1 is integrated over a dissociation probability determined from the set of ro-vibrational frequencies appropriate for the energized molecule and the transition state (TS) leading to dissociation. Choices for the molecular parameters of the TS can be estimated with two limiting assumptions and a choice that reflects the most probable TS. The first limit is to ignore the lifetime effect entirely. (In essence, this assumes that the rate of dissociation is always faster than the experimental time scale.) An upper limit to the kinetic shift is provided by a tight TS, where the molecular parameters of the TS are assumed to equal those of the dissociating molecule minus the single mode that corresponds to the reaction coordinate. The reaction coordinate, identified by boldface type in Table 1, is associated with a Li−O stretch. Because the interactions between the lithium ion and the water molecules are largely electrostatic, the most appropriate model for estimating the lifetime effect should be a loose transition state. Therefore, most of the molecular parameters of the loose TS used in these calculations are just the vibrational frequencies of the products and can be taken from Table 1. The transitional frequencies, those that become rotations and translations of the completely dissociated products, are treated as rotors, a treatment that corresponds to a phase space limit (PSL) and is described in detail elsewhere.[3] Briefly, two of the rotors are simply the rotational constants of the H_2O product (9.28 and 27.79 cm^{-1}), those with axes that are perpendicular to the reaction coordinate. In the $Li^+(H_2O)$ system, which yields one atomic product, these are the only two transitional modes. For the larger clusters, three additional transitional modes exist. Two of these rotors are the rotational constants of the $Li^+(H_2O)_{n-1}$ product, again those that are perpendicular to the reaction coordinate. Of the two rotational constants of the products with axes lying along the reaction coordinate, one is a transitional mode and is assigned as the remaining rotational constant of the H_2O product (14.50 cm^{-1}). The other becomes the 1-D external rotor of the TS. The 2-D external rotor of the TS is calculated by assuming that the TS occurs at the centrifugal barrier for interaction of the cluster ion with H_2O, using formulas listed by Khan et al.[1] that are based on a treatment of Waage and Rabinovitch.[38] The geometry of the dissociating $Li^+(H_2O)_n$ cluster is then adjusted to include this extended cluster−H_2O bond distance and the 2-D rotational constant calculated. It is also verified that this has little or no effect on the 1-D rotational constant (that having an axis parallel to the extended bond, the reaction coordinate). The 2-D external rotations are treated adiabatically but with centrifugal effects included consistent with the discussion of Waage and Rabinovitch,[38] although statistical assumptions appropriate for collisional activation are included. These are discussed in detail elsewhere.[3] More recent developments concerning this lifetime analysis suggest the use of a variationally determined TS and associated rotational constants, but the effects of this change on the thresholds have been found to be less than ~0.01 eV, much less than the typical experimental error.[3]

The model represented by eq 1 is expected to be appropriate for translationally driven reactions.[39] This model form has been

found to reproduce reaction cross sections well in a number of previous studies of both atom−diatom and polyatomic reactions,[40,41] including CID processes.[1,10,29,30] The model is convoluted with the kinetic energy distribution of the reactants, and a nonlinear least-squares analysis of the data is performed to give optimized values for the parameters σ_0, E_0, and n. The error associated with the measurement of E_0 is estimated from the range of threshold values determined for different data sets, variations associated with uncertainties in the vibrational frequencies, and the error in the absolute energy scale, 0.05 eV (Lab). Because the calculations performed by FGKP on $Li^+(H_2O)_n$, $n = 1-6$, were carried out at varying levels of theory, our estimates of the uncertainties in their calculated vibrational frequencies also varied. For $n = 1-3$, the MP2 frequencies were used directly with estimated uncertainties obtained by scaling the frequencies by factors of 0.9 and 1.1. For $n = 4-6$, the RHF frequencies were scaled by 0.9 before use and uncertainties estimated by using scaling factors of 0.7 and 1.1. These scaling procedures were used to determine the average vibrational energies of all clusters, as listed in Table 1, with the change in the average vibrational energy upon scaling by the different factors taken to be one standard deviation of the uncertainty in vibrational energy. For analyses that include the RRKM lifetime effect, the uncertainties in the reported E_0 values also include the effects of increasing and decreasing the time assumed available for dissociation (10^{-4} s) by a factor of 2 and the sensitivity of our analysis to the values used for the transitional modes (by multiplying and dividing the rotational constants for these 1-D rotors by a factor of 2). Uncertainties associated with our choices for the external rotational constants of the TS were also included. Upper limits to these values were obtained by setting them equal to those of the energized molecule, and lower limits were estimated by dividing the rotational constants used for the TS by a factor of 10.

Equation 1 explicitly includes the internal energy of the ion, E_i. All energy available is treated statistically, which should be a reasonable assumption because the internal energy of the reactants is redistributed throughout the ion upon impact with the collision gas. The threshold for dissociation is by definition the minimum energy required to lead to dissociation and thus corresponds to formation of products with no internal excitation. The assumption that products formed at threshold have an internal temperature of 0 K has been tested for several systems,[1,2,10,29,30] where it has been shown that treating all energy of the ion, vibrational, rotational, and translational, as capable of coupling into the dissociation coordinate leads to reasonable thermochemistry. The threshold energies for dissociation reactions determined by analysis with eq 1 are converted to 0 K BDEs by assuming that E_0 represents the energy difference between reactants and products at 0 K.[42] This requires that there are no activation barriers in excess of the endothermicity of dissociation. This is generally true for ion−molecule reactions[40] and should be valid for the simple bond fission reactions examined here.[43]

To compare bond energies measured here with those determined in the literature, 0 K BDEs are converted to 298 K enthalpies. The enthalpies of a nonlinear polyatomic molecule at some temperature T are related to those at 0 K by the following relationship[44]

$$[H^o_0 - H^o_T] \approx -4RT - RT\sum_i u_i/(e^{u_i} - 1) \qquad (2)$$

where the summation is carried out over all of the vibrational frequencies of the polyatomic molecule, ν_i, and $u_i = h\nu_i/k_BT$. Using the above expression, dissociation enthalpies for $Li^+(H_2O)_n$, $n = 1-6$, at 298 K are obtained by adding 4.1, 1.2, 1.0, 1.9, 3.4, and 2.6 kJ/mol, respectively, to the 0 K BDEs.

Results

Experimental cross sections are shown in Figure 1 for the interaction of $Li^+(H_2O)_n$, $n = 1-6$, clusters with Xe. The sequential loss of intact water molecules and ligand exchange with xenon are the only processes observed in these systems over the collision energy range studied, typically 0 to >5 eV. The primary (most favorable) process for all complexes is the loss of a single water molecule in the collision-induced dissociation (CID) reaction 3.

$$Li^+(H_2O)_n + Xe \rightarrow Li^+(H_2O)_{n-1} + H_2O + Xe \qquad (3)$$

As the size of the cluster increases, the maximum cross section for reaction 3 (as well as the total cross section) increases in magnitude in a manner consistent with the percentage increase in ligands, except for the case of $Li^+(H_2O)_5$. Here, the cross section increases by 70%, an effect that we attribute to the fifth water molecule being in the second solvent shell.[23] As the size of the cluster increases, the threshold for reaction 3 decreases, consistent with conventional ideas of ligation of gas-phase ions; i.e., stepwise sequential bond energies decrease because of increasing electrostatic repulsion between the ligands, causing the distance between the cation and ligands to increase. Such ideas have been noted in previous experimental and theoretical studies of $M^+(H_2O)_n$ complexes.[5,12,23]

Dissociation of additional H_2O ligands is observed for the larger clusters. For $n \geq 2$, loss of a second water molecule is observed at higher energies. For $n \geq 4$, loss of a third water molecule is observed at even higher energies. As the size of the cluster increases, secondary and tertiary dissociation account for increasingly greater percentages of the total cross section, approximately 3, 25, 45, 52, and 62% for $n = 2-6$, respectively, at the highest energies examined.

The cross sections for ligand exchange decrease as the size of the clusters increase. For the case of $n = 1$, the cross section for the ligand exchange process is substantial, having a maximum nearly as large as the CID process. For the $n = 2$ cluster, the ligand exchange cross section has dropped by an order of magnitude. For larger clusters, the efficiencies of the ligand exchange processes drop off rapidly enough that they could not be measured for clusters with greater than three water molecules.

$Li^+(H_2O)$ + Xe. Results for the interaction of $Li^+(H_2O)$ with xenon are shown in Figure 1a. This system was the most problematic of all systems studied here and more challenging than most systems we have studied by CID in the past. This is largely because it is difficult to routinely achieve efficient collection of the very light mass of the Li^+ product. Twelve independent data sets were obtained over the course of 6 months, and the agreement between the results was satisfactory (magnitudes within the 50% absolute error) but not excellent. The major product is Li^+, which has an apparent threshold below 1 eV and a maximum cross section of ~4 Å^2. The ligand exchange product Li^+Xe is observed with an apparent threshold near 0.5 eV and a maximum cross section of ~2.3 Å^2 at 2.5 eV, which drops off rapidly with energy due to competition with the primary CID process. Because the Li^+Xe ligand exchange product cross section has a lower threshold than the Li^+ product and an appreciable magnitude, it seems plausible that the apparent threshold for the CID process may be shifted to energies higher than the true thermodynamic threshold by

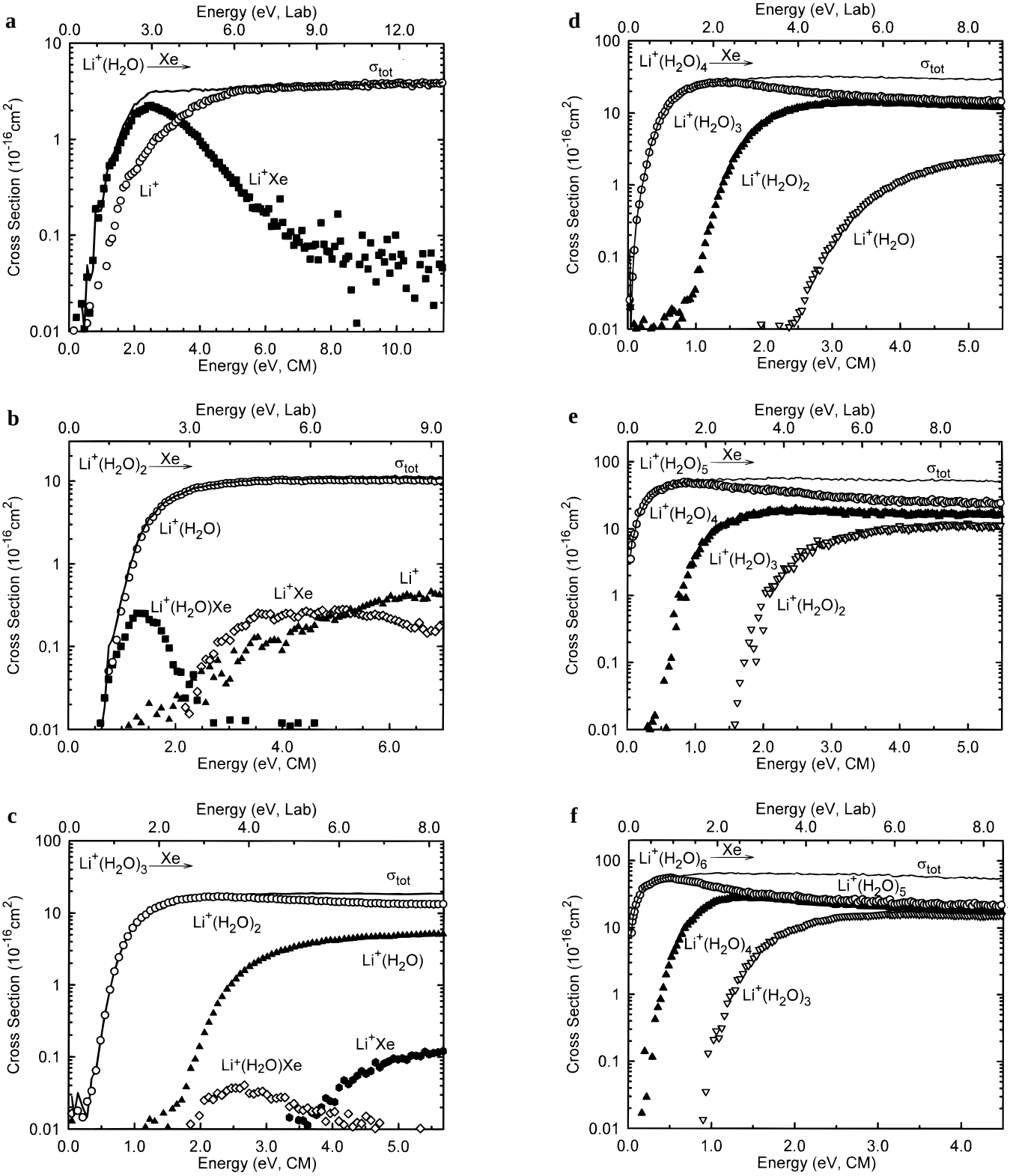

Figure 1. Cross sections for CID of $Li^+(H_2O)_n$, $n = 1-6$ (parts a−f, respectively), as a function of kinetic energy in the center-of-mass frame (lower *x* axis) and the laboratory frame (upper *x* axis). Open circles show the primary cross sections extrapolated to zero pressure of the Xe reactant. Filled triangles and open inverted triangles show the secondary and tertiary product cross sections, respectively. Closed squares, open diamonds, and closed hexagons show the primary, secondary, and tertiary ligand exchange product cross sections, respectively.

competition with this ligand exchange process, a competitive shift. We do not believe that this is a problem in this system as the threshold measured here for the CID process is lower than previously reported dissociation enthalpies for this system, as will be discussed below.

A more subtle effect is the possibility of both direct (reaction 4a) and indirect (reaction 4b) pathways for production of Li^+.

$$Li^+(H_2O) + Xe \rightarrow Li^+(H_2O)^* + Xe \rightarrow Li^+ + H_2O + Xe \quad (4a)$$

$$\rightarrow Li^+(Xe)^* + H_2O \rightarrow Li^+ + H_2O + Xe \quad (4b)$$

Although the overall energetics of these two processes are

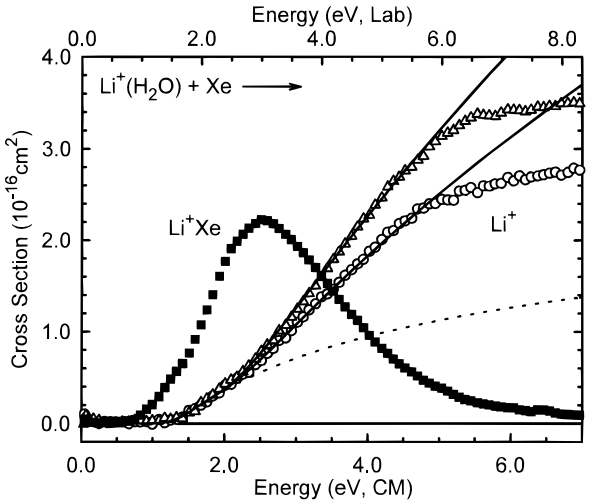

Figure 2. Cross sections for CID of $Li^+(H_2O)$ in the threshold region as a function of kinetic energy in the center-of-mass frame (lower *x* axis) and the laboratory frame (upper *x* axis). Open symbols show two independent data sets for the Li^+ product cross sections while the closed symbols show data for the Li^+Xe ligand exchange product cross sections. The dotted line shows the model cross section for the direct CID process, reaction 4a, starting at 1.33 eV after convolution over the neutral and ion kinetic and internal energy distributions. The solid lines show the sum of this model with one for the indirect CID process, reaction 4b, starting at 2.1 eV after convolution over the neutral and ion kinetic and internal energy distributions. The latter two models differ only in the magnitude of the indirect CID process.

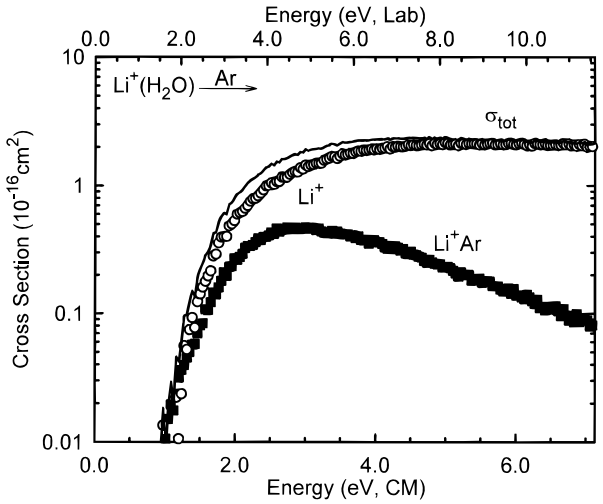

Figure 3. Cross sections for CID of $Li^+(H_2O)$ as a function of kinetic energy in the center-of-mass frame (lower *x* axis) and the laboratory frame (upper *x* axis). Open circles show the primary cross sections extrapolated to zero pressure of the Ar reactant. Closed squares show the primary ligand exchange product cross sections.

identical, the dynamics and energy distributions of the two channels may differ appreciably. Some evidence for two pathways comes from replicate sets of data for the $Li^+(H_2O)$ + Xe interaction, as shown in Figure 2. The Li^+ cross sections were obtained under slightly different focusing conditions. The Li^+Xe cross section was obtained at the same time as the higher Li^+ cross section. (Unfortunately, this product was not collected in the data set for the lower Li^+ cross section.) It can be seen that the two Li^+ cross sections agree precisely up to about 2.3 eV, at which point they begin to deviate. Such deviations can be the result of somewhat different collection efficiencies for different focusing conditions. This behavior is consistent with a low-energy process (having collision dynamics such that the collection efficiency is unaffected by focusing) and a higher energy process that begins near 2 eV. Note that the deviation between the two Li^+ cross sections begins at about the same energy as the peak in the Li^+Xe cross section, identifying the higher energy process as indirect CID, reaction 4b. Clearly, appreciable contributions to the Li^+ cross section from two pathways will complicate the threshold analysis, as discussed further below.

$Li^+(H_2O)$ + Ar. We can experimentally test whether both the direct and indirect CID pathways occur by examining the CID of the $Li^+(H_2O)$ complex with a collision gas that has a much lower probability of undergoing the ligand exchange reaction analogous to process 4b. Any of the lighter rare gases would suffice, with the additional concern that the translational to internal energy transfer needed to induce dissociation of the complex will be less efficient. Results for reaction of $Li^+(H_2O)$ with Ar are shown in Figure 3. Clearly, the ligand exchange process is severely reduced. Further, the CID cross section has a magnitude comparable to that for the Xe data at lower energies, but does not increase to the same magnitude at elevated energies. This is consistent with a high-energy contribution from indirect CID in the case of Xe. Finally, we note that the apparent threshold for CID is somewhat higher in the Ar data than for the Xe collision partner, consistent with less efficient energy transfer. Overall, we conclude that the indirect CID pathway is definitely operative for the Xe collision gas. The consequences of this contribution are explored further in the data analysis section below.

$Li^+(H_2O)_n$, $n = 2-6$. The CID results for doubly hydrated Li^+ are shown in Figure 1b. The loss of one water molecule from this species begins at an apparent threshold near 0.7 eV with a cross section that is more than twice as large as that of the monohydrated ion. The secondary product of this reaction, Li^+, has an apparent threshold of ~2 eV. At lower energies, there is a nonzero base line which is believed to be an artifact of the collection efficiency of the low mass combined with the small inherent signal for this secondary process. Two ligand exchange products are observed, $Li^+(H_2O)Xe$ and Li^+Xe. The primary ligand exchange product, $Li^+(H_2O)Xe$, rises from an apparent threshold near 0.6 eV to a maximum of 0.3 Å^2 at approximately 1.3 eV. At higher energies, it falls off rapidly due to competition with the primary CID process. The secondary ligand exchange product, Li^+Xe, slowly grows in from an apparent threshold near 2 eV to a maximum of 0.25 Å^2 at approximately 5 eV.

The CID pattern for triply hydrated Li^+ (Figure 1c) is notably different from the doubly hydrated ion. The apparent threshold of the primary product, $Li^+(H_2O)_2$, occurs at 0.4 eV with a cross section that is again approximately twice as large at its maximum as the maximum observed for the loss of one water molecule from the doubly hydrated ion. The cross section for production of the primary product decreases as the secondary $Li^+(H_2O)$ product appears. The threshold for the secondary product appears at ~1.5 eV with a maximum cross section of ~5 Å^2. Formation of the tertiary product, Li^+, which is not expected to be an efficient process, is not observed even at higher energies, although this may be partially attributable to low collection efficiency. Again, two ligand exchange products are observed. The primary ligand exchange product, $Li^+(H_2O)_2Xe$, is not observed. The secondary ligand exchange product, $Li^+(H_2O)Xe$, rises from an apparent threshold near 1.8 eV to a maximum cross section of 0.05 Å^2. At ~2.7 eV, the cross section for the secondary ligand exchange product begins to drop off as the tertiary ligand exchange product, Li^+Xe, grows in. The apparent threshold for Li^+Xe appears at ~3.2 eV with a maximum cross section of 0.1 Å^2.

TABLE 3: Summary of Parameters of Eq 1 for Modeling Primary H_2O Loss from $Li^+(H_2O)_n$, $n = 1-6$, and Entropies of Activation[a]

species	σ_0[b]	n[b]	E_0[c] (eV)	E_0(loose) (eV)	$\Delta S^\dagger$(loose)[d] (J/(mol K))	E_0(tight) (eV)	$\Delta S^\dagger$(tight)[d] (J/(mol K))
$Li^+(H_2O)$	1.75 (0.41)[e]	1.0−1.4[e]	1.33 (0.16)[e]	1.33 (0.16)[e]	31 (27)	1.33 (0.16)[e]	−11
	1.56 (0.47)	1.76 (0.16)	1.20 (0.12)	1.20 (0.12)		1.20 (0.12)	
	2.08 (0.06)[f]	1.38 (0.03)[f]	1.48 (0.05)[f]	1.48 (0.05)[f]		1.48 (0.05)[f]	
$Li^+(H_2O)_2$	13.46 (1.02)	1.31 (0.11)	1.17 (0.10)	1.17 (0.10)	42 (28)	1.16 (0.09)	−8
$Li^+(H_2O)_3$	26.47 (0.65)	0.95 (0.04)	0.99 (0.05)	0.97 (0.04)	42 (27)	0.90 (0.04)	−5
$Li^+(H_2O)_4$	38.93 (1.78)[g]	0.95 (0.02)[g]	0.74 (0.05)[g]	0.72 (0.05)[g]	51 (33)	0.63 (0.05)[g]	−1
	38.56 (1.66)[h]	0.91 (0.06)[h]	0.75 (0.05)[h]	0.73 (0.05)[h]		0.63 (0.05)[h]	
$Li^+(H_2O)_5$	56.05 (16.15)[g]	1.00 (0.13)[g]	0.62 (0.05)[g]	0.59 (0.04)[g]	79 (25)	0.45 (0.04)[g]	−8
	69.75 (37.43)[h]	1.38 (0.12)[h]	0.52 (0.06)[h]	0.50 (0.05)[h]		0.38 (0.04)[h]	
$Li^+(H_2O)_6$	75.54 (3.03)[g]	0.88 (0.03)[g]	0.70 (0.08)[g]	0.62 (0.05)[g]	103 (27)	0.40 (0.04)[g]	−5
	300.35(72.46)[h]	1.35 (0.10)[h]	0.69 (0.08)[h]	0.63 (0.03)[h]		0.33 (0.04)[h]	

[a] Uncertainties are listed in parentheses. [b] Average values for loose transition state. [c] No RRKM analysis. [d] $\Delta S^\dagger$ is calculated at 1000 K. [e] Values obtained when the data are analyzed including consideration of the indirect CID pathway, reaction 4b. Values of n are restricted to the range noted. [f] Values obtained when the data obtained using Ar as the collision gas is analyzed. [g] Average values obtained when fitting the total cross section. [h] Average values obtained when fitting the channel corresponding to the loss of one water molecule.

The CID pattern of quadruply hydrated Li^+ shown in Figure 1d is similar to that observed for the triply hydrated ion, except that at higher energies the secondary and tertiary dissociation processes account for a greater percentage of the total cross section. The apparent threshold of the primary product, $Li^+(H_2O)_3$, appears at ~0.1 eV with a cross section that is ~50% greater than the triply hydrated species at their respective maxima. The primary cross section declines slightly more rapidly than for the triply hydrated species beginning at the apparent threshold of the secondary $Li^+(H_2O)_2$ product, which appears at ~1 eV. This product reaches a maximum cross section of ~14 Å^2 and then drops off slowly as the tertiary product, $Li^+(H_2O)$, grows in from an apparent threshold near 2.5 eV. The $Li^+(H_2O)$ product reaches a maximum cross section of ~3 Å^2 at the highest energies examined. Again, the Li^+ product is not observed. The ligand exchange product channels were again monitored, however, signals were sufficiently small that they were not discernible from noise.

The CID pattern of the quintuply hydrated Li^+, shown in Figure 1e, is again similar to that observed for the complex containing one fewer water molecule. The primary product, $Li^+(H_2O)_4$, rises from an apparent threshold near 0 eV with a cross section that is ~70% greater than that of the quadruply hydrated species at their respective maxima, as noted above. The primary cross section declines slightly more rapidly than for the quadruply hydrated species beginning at the apparent threshold of the secondary $Li^+(H_2O)_3$ product, which appears at ~0.5 eV. This product reaches a maximum cross section of ~18 Å^2 and then drops off slightly as the tertiary product, $Li^+(H_2O)_2$, grows in from an apparent threshold near 1.7 eV. The $Li^+(H_2O)_2$ product reaches a maximum cross section of ~12 Å^2 at the highest energies examined. The $Li^+(H_2O)$ and Li^+ products, which are not expected to be formed very efficiently, are not observed over the range of energies examined. The ligand exchange product channels were again too small to detect.

The CID pattern of sextuply hydrated Li^+, shown in Figure 1f, is very similar to that for $Li^+(H_2O)_5$. The primary product, $Li^+(H_2O)_5$, rises from an apparent threshold near 0 eV with a cross section that is ~20% greater than that of the quintuply hydrated species at the respective maxima. The primary cross section declines slightly more rapidly than in the quintuply hydrated species beginning at the apparent threshold of the secondary $Li^+(H_2O)_4$ product, which appears at ~0.3 eV. This product reaches a maximum cross section of ~28 Å^2 and then drops off slowly as the tertiary product, $Li^+(H_2O)_3$, grows in from an apparent threshold near 0.9 eV. The $Li^+(H_2O)_3$ product reaches a maximum cross section of ~15 Å^2 at the highest energies examined. The $Li^+(H_2O)_2$, $Li^+(H_2O)$, Li^+, and ligand exchange products, which are not expected to be formed very efficiently, are not observed over the range of energies examined.

Threshold Analysis. The model represented by eq 1 was used to analyze the thresholds for reaction 3 in all six $Li^+(H_2O)_n$ systems. As previously discussed,[1,29,30] we believe the analysis of the primary CID thresholds provides the most reliable thermochemistry from such studies. This is because secondary and higher order products are more sensitive to lifetime effects, and additional assumptions are needed to quantitatively include the multiple products formed. The results of these analyses are provided in Table 3 along with entropies of activation, a measure of the tightness or looseness of the transition state. Three values of E_0 are listed: one without the RRKM lifetime analysis and two where the lifetime analysis is included (a loose PSL and a tight TS model). As noted above, the values obtained with no RRKM analysis should be conservative upper limits to the true thermodynamic thresholds, while those using a tight TS provide a conservative lower limits. Comparison of these three E_0 values shows that the kinetic shifts are relatively small and increase with the number of water molecules surrounding the lithium ion. Thus, dissociation of $Li^+(H_2O)$ shows no kinetic shift (even when a tight TS is used), while $Li^+(H_2O)_6$ exhibits a kinetic shift of approximately 0.07 eV when calculated with a loose PSL TS and 0.3 eV when calculated with a tight TS. Our most accurate experimental values are expected to come from the loose PSL TS model, an assumption that has been tested in several systems previously.[2,45,46] This conclusion will be tested further here by comparison of these values with the results of DK[5] below.

Experimental cross sections and fits to the data using a loose PSL TS model are shown in Figure 4 for loss of a single water molecule in the interaction of $Li^+(H_2O)_n$, $n = 1-6$, clusters with Xe (reaction 3) and $Li^+(H_2O)$ with Ar. For $n = 1-4$, it can be seen that the fits reproduce the data well over an energy range exceeding 1 eV and magnitudes of at least a factor of 100. For the $n = 5$ and 6 clusters, the cross sections are still finite at the lowest energies we examine, and hence the reproduction does not cover the same magnitude range.

Two values for each of the three lifetime models (no RRKM, loose PSL, and tight TSs) are listed in Table 3 for the $Li^+(H_2O)_n$, $n = 4-6$, clusters. These represent analysis of the *total* cross section for dissociation and an analysis of the cross section for loss of a single water molecule. In order to reproduce the shapes of the latter cross sections over an extended energy range, the effects of subsequent water loss need to be included in the

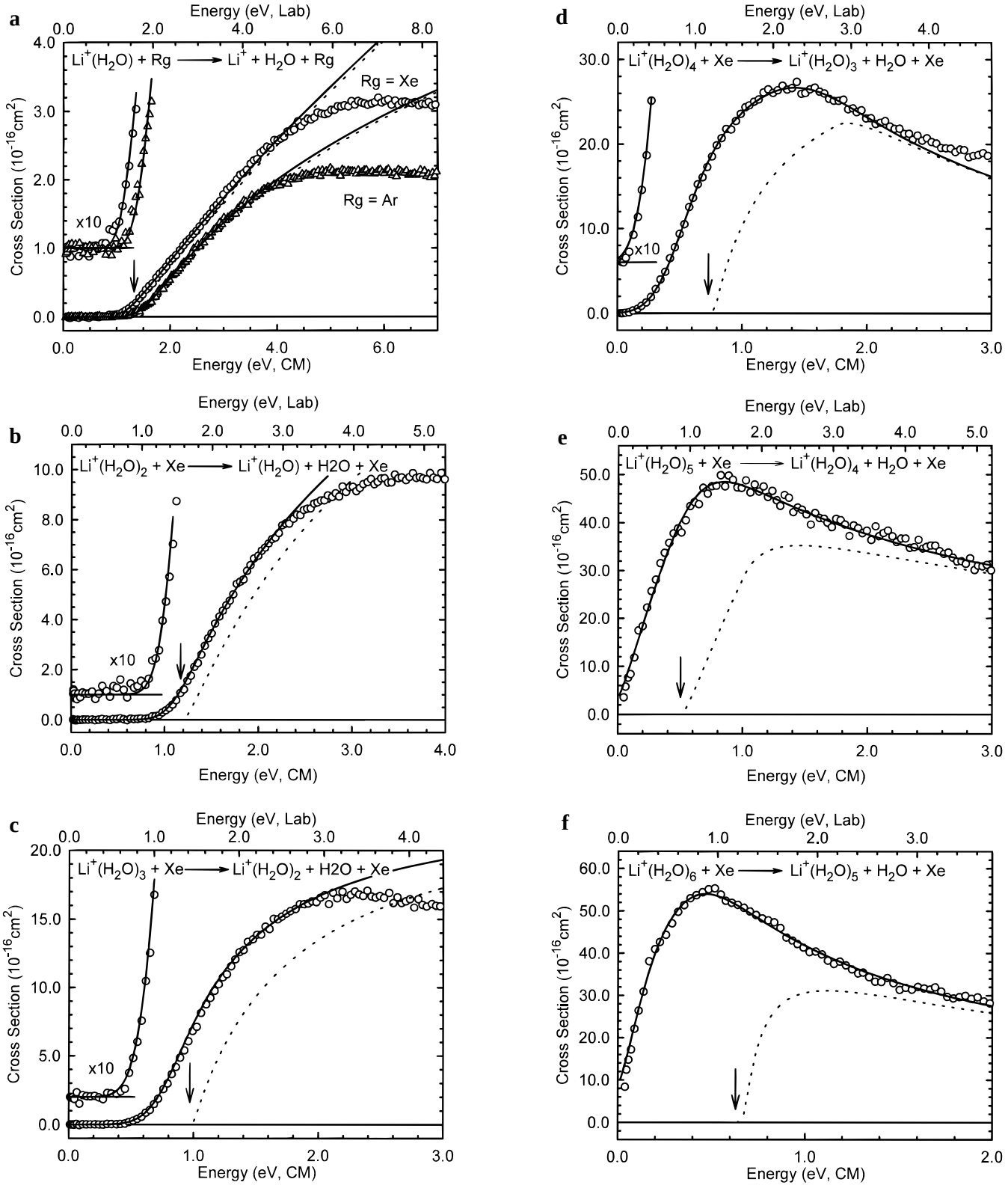

Figure 4. Cross sections for CID of $Li^+(H_2O)_n$, $n = 1-6$ (parts a−f, respectively), in the threshold region as a function of kinetic energy in the center-of-mass frame (lower *x* axis) and the laboratory frame (upper *x* axis). Open circles show the primary cross sections extrapolated to zero pressure of the Xe reactant. Part a shows the primary cross sections extrapolated to zero pressure of the Ar reactant as open triangles. The best fits to the data using the model of eq 1 convoluted over the neutral and ion kinetic and internal energy distributions are shown as solid lines. Dotted lines show the model cross sections in the absence of experimental kinetic energy broadening for reactants with an internal energy of 0 K. Average threshold energies are indicated by arrows.

analysis. This is achieved by using a simple statistical model that conserves angular momentum, as described in detail previously.[47] This model depends on E_D, the energy at which the dissociation channel begins, and *p*, a parameter similar to *n* in eq 1. Experimental cross sections and fits to the total CID cross sections using a loose PSL TS model are shown in Figure 5 for the interaction of $Li^+(H_2O)_n$, $n = 4-6$, clusters with Xe. For the $n = 1-3$ clusters, these two models give identical results, while nearly identical results are obtained for the $n = 4$ cluster. For the larger clusters, $n = 5$ and 6, the thresholds

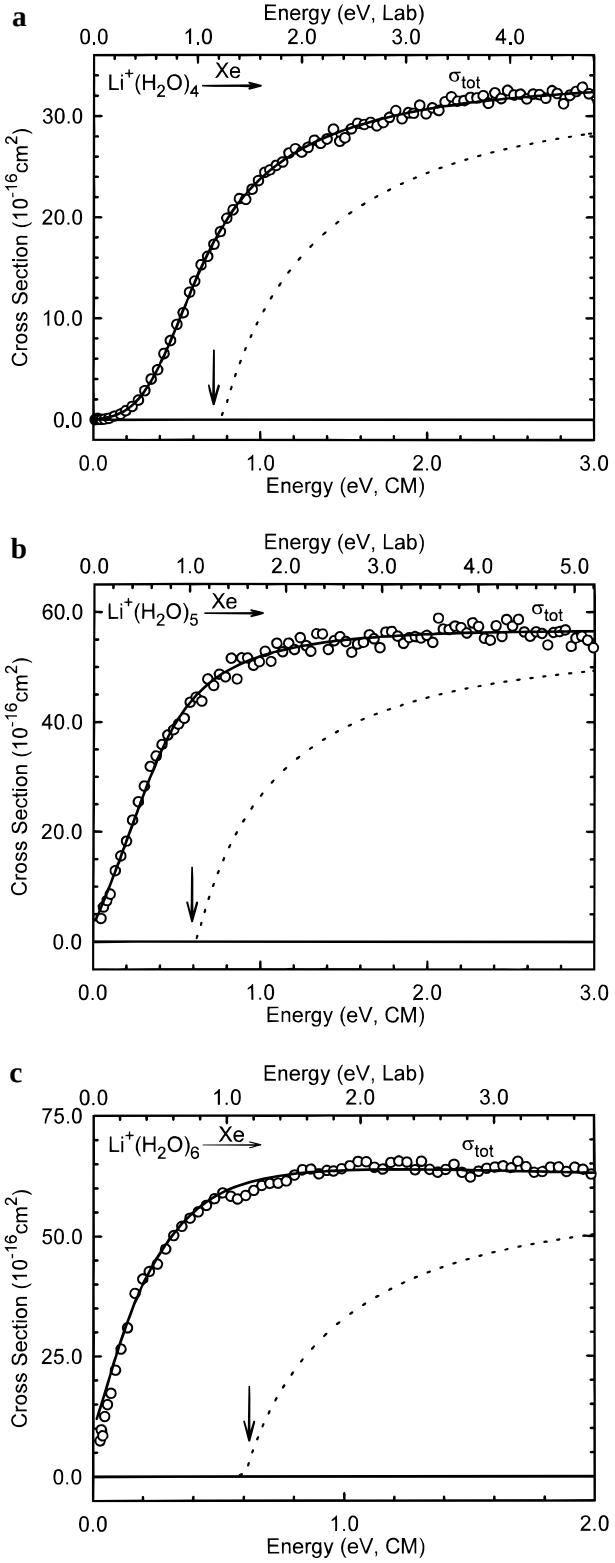

Figure 5. Cross sections for CID of $Li^+(H_2O)_n$, $n = 4-6$ (parts a−c, respectively), in the threshold region as a function of kinetic energy in the center-of-mass frame (lower *x* axis) and the laboratory frame (upper *x* axis). Open circles show the total cross section (σ_{tot}) extrapolated to zero pressure of the Xe reactant. The best fits to the data using the model of eq 1 convoluted over the neutral and ion kinetic and internal energy distributions are shown as solid lines. The dotted lines show the model cross sections in the absence of experimental kinetic energy broadening for reactants with an internal energy of 0 K. Threshold energies are indicated by arrows.

obtained using the two models differ by between 0.01 and 0.10 eV. In these systems, the cross sections for reaction 3 are strongly affected by subsequent dissociation shortly after the threshold, such that the energy range unaffected by this second-order process is narrow. Although the high-energy model has proven to be extremely useful in describing such subsequent dissociations, it is not designed to include lifetime effects in such dissociations. Because such effects could be appreciable in the $n = 4-6$ clusters, the reliability of the analyses that include this simple high-energy model is unclear. Using this high-energy model, the fits to the data show deviations at the highest energies (typically beginning at an energy where the secondary CID process becomes substantial) because this model does not account for the distribution of energies that the departing H_2O carries off. When the total cross section is analyzed, the data can be reproduced over a wider energy range. Therefore, we believe the results obtained by reproducing the total cross sections are probably more accurate.

For the case of $Li^+(H_2O)$, we also need to consider how the competing reactions 4a and 4b might influence the threshold analysis. Presuming that the indirect CID process changes the shape of the Li^+ cross section starting near 2 eV, we analyzed the data only below this energy. Because the range over which the data were analyzed was so limited, it was necessary to restrict the parameter *n* to values consistent with other systems, such that a range of $n = 1.0-1.4$ was chosen (see Table 3). The threshold measured for the Li^+ product shifts to higher energies, Table 3, because a lower value of *n* is used to reproduce the threshold region. The higher energy process can be reproduced by subtracting the two data sets shown in Figure 2 from one another and modeling the difference. This analysis of the high-energy portion of the cross sections (the indirect CID process) gives parameters in eq 1 of $E_0 = 2.1$ eV, $n = 1.7$, and a value of σ_0 that varies between data sets. Overall, the entire cross section curves can now be reproduced using sums of these two models, as shown in Figure 2.

The complicated analysis for the $Li^+(H_2O)$ complex can also be checked by analyzing the data for reaction of $Li^+(H_2O)$ with Ar where the indirect CID pathway is greatly reduced. As shown in Figure 4a, this data is accurately reproduced over an extended range of energies with a value of *n* (1.4) consistent with the larger complexes. The threshold for the Ar data is higher than that for either interpretation of the Xe data (Table 3). It should be noted that the comparison of the Ar and Xe data on the linear scales of Figures 2 and 4a makes the contribution of the indirect pathway more evident. Figure 4a shows that the $Li^+(H_2O)$ CID cross sections in the two systems are similar in magnitude at low energies (up to about 3 eV), but diverge more strongly at higher energies. This is consistent with the varying magnitudes in the Xe cross sections, as shown in Figure 2.

Discussion

Our experimental results (determined with threshold analyses corrected for lifetime effects assuming a loose PSL transition state) converted to BDEs at 298 K of $Li^+(H_2O)_n$, $n = 1-6$, are compared with previous experimental and theoretical values in Table 4. Values for $n = 4-6$ are those determined from analysis of total cross section data (although this makes a difference only in the case of $n = 5$). Because the value for $Li^+(H_2O)$ reported by DK is extrapolated rather than measured, this value is discussed separately, as will the value for the largest cluster studied here, $Li^+(H_2O)_6$.

$Li^+(H_2O)_n$, $n = 2-5$. Our results for $Li^+(H_2O)_n$, $n = 2-5$, are within experimental error of the earlier values obtained by DK, as can be seen in Figure 6. The average deviation between these experimental determinations is 4 ± 3 kJ/mol, well within the experimental uncertainties of either measurement. The

TABLE 4: Bond Dissociation Enthalpies of $Li^+(H_2O)_n$, $n = 1-6$, at 298 K in kJ/mol[a]

species	ΔH_{298}(expt)[b]	ΔH_{298}(DK)[f]	ΔH_{298}(theory)[g]
$Li^+(H_2O)$	137(14)[c,d]	142(4)	135,[g] 136[h]
$Li^+(H_2O)_2$	114(10)[c]	108(4)	114[g]
$Li^+(H_2O)_3$	94(4)[c]	87(4)	91[g]
$Li^+(H_2O)_4$	71(5)[e]	69(4)	67[g]
$Li^+(H_2O)_5$	60(4)[e]	58(4)	55[g]
$Li^+(H_2O)_6$	63(5)[e]	51(4)	44[g]

[a] Uncertainties are listed in parentheses. [b] Loose transition state values taken from Table 3. [c] The enthalpy corrections are determined using MP2 harmonic frequencies. [d] Average of Ar and Xe results (when Xe data are analyzed including consideration of the indirect CID process, reaction 4b). [e] The enthalpy corrections are determined using RHF harmonic frequencies scaled by 0.9. [f] Reference 5. [g] MP2 values taken from ref 23. [h] Average value obtained in ref 21 using varying levels of correlation at the MP2/6-31+G(2d, 2p) level.

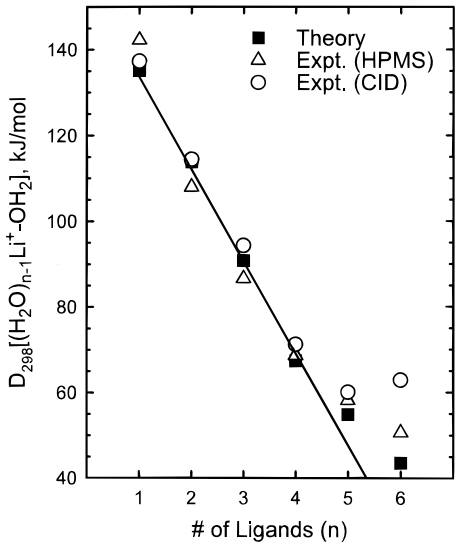

Figure 6. Bond energies at 298 K (in kJ/mol) of $[(H_2O)_{n-1}Li^+-OH_2]$ plotted versus *n*. Experimental HPMS and theoretical bond energies are taken from refs 5 and 23, respectively.

agreement between theory and the present results for these four clusters is also very good, Figure 6, with our experimental values being slightly higher by an average of 3 ± 2 kJ/mol. Absolute deviations between theory and DK's values are 4 ± 2 kJ/mol.

It is also worth checking our assumption that the loose PSL TS model provides the most accurate results. This can be achieved by comparing the values obtained without the RRKM analysis and with the tight TS model to the literature thermochemistry. The values with no RRKM analysis are fairly close to those of the loose PSL TS model; hence, the deviations from the values of DK and theory are only slightly higher, 6 ± 2 and 5 ± 3 kJ/mol, respectively. Most of the tight TS values are now *lower* than the literature enthalpies by averages of 6 ± 4 and 4 ± 3 kJ/mol, respectively. Overall, because the kinetic shifts calculated for the lithium−water ion clusters are not very large, this system does not provide a very sensitive test for the different lifetime models. As the threshold energies determined with a loose PSL TS are central to the upper and lower limits provided by alternate assumptions, these can still be regarded as our best determinations.

$Li^+(H_2O)_6$. Our results for $Li^+(H_2O)_6$ are not in good agreement with either the value measured by DK or the calculated value (Table 4 and Figure 6). Although some of this discrepancy could be eliminated by using a tighter transition state, then the agreement among the different determinations would be worse for smaller clusters, particularly $n = 5$. It is conceivable that the BDEs for $Li^+(H_2O)_n$, $n = 5$ and 6, should be fairly similar. The geometries of these clusters as calculated by FGKP[23] show that the fifth and sixth water ligands are bound in the second solvation shell by hydrogen-bonding interactions to two of the water ligands in the first solvation shell. Thus, the interactions of the fifth and sixth ligand with the $Li^+(H_2O)_4$ cluster might be expected to be comparable. Additional evidence for this near equality comes from experimental studies of proton bound water clusters, $H^+(H_2O)_n$, where the fifth and sixth water ligands also begin the second solvation shell. Three separate studies (both HPMS[48,49] and CID[30] experiments) find that the bond energies for the $n = 5$ and 6 proton bound clusters are nearly equal, average values of 52 ± 3 and 49 ± 2 kJ/mol, respectively, with experimental uncertainties in both numbers of approximately 4 kJ/mol. A similar equivalency was determined by Magnera, David, and Michl[50] although the bond energies determined in this work are not in quantitative agreement with the other three studies. Further, these authors determine that the bond dissociation energies for larger clusters, $n \geq 7$, reach a fairly constant value just smaller than that for the $n = 5$ and 6 clusters. Based on these studies, there should be no firm expectation that the dissociation enthalpies for $Li^+(H_2O)_n$ clusters should decline with increasing *n*, such that the behavior observed here (equivalent bond energies within experimental error for $n = 5$ and 6) is reasonable. With regard to the difference between the trends observed here and in the theoretical calculations, it should be realized that the calculations become increasingly difficult as the size of the system increases. For the $n = 1-5$ clusters, the geometries were optimized at high levels of theory. For $n = 6$, geometries were optimized only at the restricted Hartree−Fock (RHF) level using a smaller basis set, while final energies were calculated with higher levels of theory (MP2). Thus, the accuracy of the theoretical value for $n = 6$ is not equivalent to those for the smaller clusters.

$Li^+(H_2O)$. When analyzed with no consideration of the indirect CID process, our bond energy is lower than the value reported by DK[5] (Table 4). The results obtained with Ar as the collision gas confirm that this analysis of the Xe data is incorrect. When the indirect CID process is taken into account in our analysis of the Xe data, the threshold is still lower but within experimental error of DK's estimate. When data obtained with Ar as a collision gas are analyzed, the threshold is slightly higher than the estimate of DK. This is consistent with Ar being a less efficient energy transfer agent[10,27,28] and could suggest that this threshold should be viewed as an upper limit to the thermodynamic threshold. Alternatively, we could average the threshold obtained with Ar as a collision gas and with Xe as long as the interpretations were equivalent. This suggests that the Xe data be evaluated with consideration of indirect CID and the value of *n* used in eq 1 is the same as the Ar system, 1.4. This leads to a threshold of 1.28 ± 0.16 eV for the Xe data, such that the average threshold is 1.38 ± 0.14 eV. This latter value is similar to that obtained by the less restrictive analysis of the Xe data (values of *n* ranging from 1.0 to 1.4), 1.33 ± 0.16 eV. Overall, we conclude that this average value is probably most representative of the correct thermodynamic threshold, a view which is partly biased by the results in the following paragraphs.

As noted in the Introduction, the bond energy for $Li^+(H_2O)$ has never been determined experimentally before. All experimental values for this bond energy used in the literature can be traced to the value reported by DK,[5] which was extrapolated from their HPMS results for larger clusters, $Li^+(H_2O)_n$, $n = 2-6$. Explicit details regarding how this extrapolation was performed were not discussed in their paper. Thus, the bond energy reported here represents the first experimental determi-

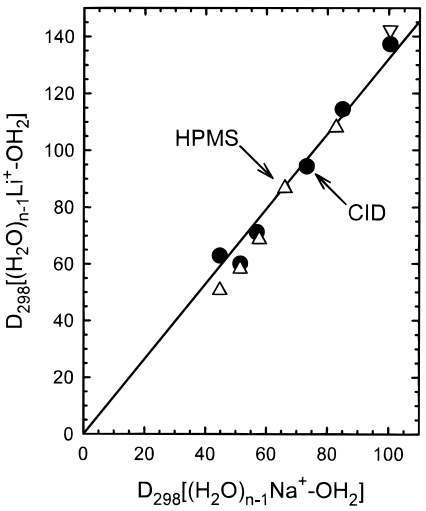

Figure 7. Bond dissociation energies at 298 K (in kJ/mol) for $[(H_2O)_{n-1}Li^+-OH_2]$ versus those for $[(H_2O)_{n-1}Na^+-OH_2]$. Closed symbols show collision-induced dissociation results from the present study and DTA (ref 12) for $n = 1-4$. (For $n = 5$ and 6, $[(H_2O)_{n-1}Na^+-OH_2]$ values are taken from ref 5.) Open symbols show HPMS results from ref 5, including the extrapolated Li^+-OH_2 value. The line is a linear regression fit through the CID data which is constrained to pass through the origin.

nation of this quantity. It is therefore important to carefully consider how reasonable this value truly is.

One means of assessing the accuracy of the $Li^+(H_2O)$ BDE is by comparison with theory. Two independent theoretical studies[21,23] performed with various basis sets and at different levels of electron correlation converge on values lying in a narrow range from 134 to 136 kJ/mol. These values (which have been properly adjusted to 298 K enthalpies) agree nicely with the present determination (Table 4 and Figure 6). The theoretical values fall below the value estimated by DK. In their study, FGKP[23] tried to remove the discrepancy between their results and DK's value by extrapolating to a complete basis set (CBS) limit. Their final CBS value agrees precisely with DK's estimate, but the accuracy and appropriateness of such an extrapolation are questionable, as noted by FGKP.[23] Hence, comparison with the bond energies actually calculated seems appropriate.

An alternative means of assessing the accuracy of our Li^+-OH_2 BDE is to perform our own extrapolation from bond energies for larger clusters. Any such treatment is inexact but may be able to address whether the high estimate of DK or which of our lower BDEs is more reasonable. A simple linear extrapolation of the data for clusters involving the first solvent shell, $n = 2-4$, predicts $D_{298}(Li^+-OH_2) = 134$ kJ/mol if data from DK, theory, and us is included, as shown in Figure 6. (A value of 128 kJ/mol is obtained from an extrapolation of DK's data alone. The theory values and ours individually extrapolate to values of 137 kJ/mol.) Any of these values are in good agreement with our average bond energy, 137 ± 14 kJ/mol. However, there is no theoretical justification for believing that the bond energies should decrease uniformly with additional ligands.

We believe that a better extrapolation approach utilizes a comparison with the analogous $Na^+(H_2O)_n$ clusters. In this system, good agreement has been obtained between bond energies measured by CID methods in our group[12] and by HPMS by DK.[5] Figure 7 shows this comparison. It is evident that a good linear correlation is obtained, although there is a legitimate question as to whether such a correlation should pass through the origin. The line shown is a linear regression analysis of the CID data constrained to pass through the origin. Very similar lines are obtained if the constraint is removed and whether or not our $n = 1$ data point is included in the correlation. Overall, these correlations can be represented by the equation $D_{298}[(H_2O)_{n-1}Li^+-OH_2] = 1.30D_{298}[(H_2O)_{n-1}Na^+-OH_2]$, such that the $D_{298}(Na^+-OH_2) = 100 \pm 8$ kJ/mol (the same value is obtained by DTA and by DK) indicates that $D_{298}(Li^+-OH_2)$ should equal 130 ± 10 kJ/mol, in excellent agreement with our experimentally determined bond energy. A linear regression analysis of the HPMS data (constrained to pass through the origin) gives a similar result, with a slope of 1.24. If the constraint is removed from the HPMS data, a very different correlation is obtained: $D_{298}[(H_2O)_{n-1}Li^+-OH_2] = 1.56D_{298}[(H_2O)_{n-1}Na^+-OH_2] - 20$. From the literature Na^+-OH_2 bond energy, this correlation predicts $D_{298}(Li^+-OH_2)$ should equal 137 ± 7 kJ/mol, again in good agreement with the present result and within experimental error of the extrapolated value of DK. Overall, these comparisons tend to suggest that the extrapolated value of DK may be slightly too high and that the present experimentally determined value for $D_{298}(Li^+-OH_2)$ is reasonable. Unfortunately, the difficulties in measuring and modeling this cross section lead to an appreciable uncertainty in our value.

To further ascertain whether it is appropriate to redefine the absolute Li^+ affinity scale, we compare the Li^+ binding energies to methanol (MeOH) and dimethyl ether (DME) that we have recently measured with those determined elsewhere.[2,46] Our values for the enthalpies of dissociation converted to 298 K values are 157 ± 9 kJ/mol for Li^+-MeOH[2] and 167 ± 10 kJ/mol for Li^+-DME.[46] Both Woodin and Beauchamp (WB) and Taft et al. performed equilibrium studies in an ion cyclotron resonance (ICR) mass spectrometer and measured the relative binding energies of Li^+ to H_2O, MeOH, and DME (as well as other molecules). WB used DK's value for $Li^+(H_2O)$ to calibrate their absolute scale, while Taft et al. took the value for $Li^+(NH_3)$ from WB to calibrate their absolute scale. WB report values of 156 ± 8 kJ/mol for Li^+-MeOH and 165 ± 8 kJ/mol for Li^+-DME using DK's value of 142 kJ/mol for Li^+-OH_2 as an anchor. The values of Taft et al. were incorrectly adjusted for their experimental temperature of 373 K. After properly adjusting their results to 298 K enthalpies and using WB's value for Li^+-DME of 165 kJ/mol as an anchor, their results yield values of 136 ± 8 kJ/mol for Li^+-OH_2 and 154 ± 8 kJ/mol for Li^+-MeOH. Clearly, all three values for Li^+ binding to MeOH and DME are in good agreement. For $Li^+(H_2O)$, our value of 137 ± 14 kJ/mol agrees nicely with that obtained from DK/WB, 142 ± 8 kJ/mol, and with that from Taft et al., 136 ± 8 kJ/mol. The latter number provides additional evidence that DK's value may be too high.

Because of the good agreement among the MeOH and DME values in the three studies, it seems reasonable to use these as accurate anchor points for a Li^+ binding affinity scale. The average of our directly determined values for $\Delta H_{298}(Li^+-OH_2)$, 137 ± 14 kJ/mol, agrees well with the extrapolated values derived above (134, 130 ± 10, and 137 ± 7 kJ/mol) and with the theory values of 134−136 kJ/mol. Overall, we conclude that there is sufficient evidence to conclude that absolute Li^+ binding affinity scales based on DK's value for Li^+-OH_2 should probably be adjusted downward by about 5 kJ/mol. However, we believe that the values we have measured elsewhere for MeOH[2] and DME[46] probably provide more accurate standards for anchoring the Li^+ affinity scale. To further pinpoint the $Li^+(H_2O)$ bond energy, we are presently investigating the CID of mixed cluster systems, such as $Li^+(H_2O)(MeOH)$. Preliminary results yield a value within experimental error of the present recommended determination.

Conclusions

Bond dissociation energies of $Li^+(H_2O)_n$, $n = 1-6$, are determined by kinetic energy-dependent collision-induced dissociation experiments in a guided ion beam mass spectrometer. Values for $Li^+(H_2O)_n$, $n = 2-5$, agree well with previous experimental and theoretical values. For $Li^+(H_2O)_6$, the present results are higher than both the experimental and theoretical values although a comparison with dissociation enthalpies for proton bound water clusters suggests that our measurement is reasonable. For $Li^+(H_2O) + Xe$, the analysis is complicated by the presence of both direct and indirect collision-induced dissociation processes as confirmed by studies of $Li^+(H_2O) + Ar$; nevertheless, the present results provide the first experimental measurement of its thermochemistry. The bond enthalpy measured here agrees well with theoretical values[21,23] and is somewhat lower than the extrapolated experimental value from Dzidic and Kebarle (DK).[5] A reanalysis of the extrapolation from larger clusters and a comparison with data for the $Na^+(H_2O)_n$ clusters lends some credence to the idea that the value of DK is slightly high. Because the absolute values of all lithium ion affinity scales can be traced back to the value estimated by DK, our new determination implies that a revision in these scales is needed. We suggest that the 298 K bond enthalpy for $Li^+(H_2O)$ should be 137 ± 14 kJ/mol, 5 kJ/mol lower than the value commonly accepted. More suitable anchor points for the Li^+ affinity scale are suggested to be bond energies to methanol or dimethyl ether.

Acknowledgment. The authors thank D. Feller and E. D. Glendening for providing access to their detailed results for the lithium ion−water clusters obtained in a previous study (ref 23). Funding for this work was provided by the National Science Foundation under Grant CHE-9530412 and by the donors of the Petroleum Research Fund, administered by the American Chemical Society.

References and Notes

(1) Khan, F. A.; Clemmer, D. C.; Schultz, R. H.; Armentrout, P. B. *J. Phys. Chem.* **1993**, *97*, 7978.
(2) Rodgers, M. T.; Armentrout, P. B. *J. Phys. Chem.*, submitted for publication.
(3) Rodgers, M. T.; Ervin, K. M.; Armentrout, P. B. *J. Chem. Phys.*, accepted for publication.
(4) Taft, R. W.; Anvia, F.; Gal, J.-F.; Walsh, S.; Capon, M.; Holmes, M. C.; Hosn, K.; Oloumi, G.; Vasanwala, R.; Yazdani, S. *Pure Appl. Chem.* **1990**, *62*, 17.
(5) Dzidic, I.; Kebarle, P. *J. Phys. Chem.* **1970**, *74*, 1466.
(6) Marinelli, P. J.; Squires, R. R. *J. Am. Chem. Soc.* **1989**, *111*, 4101.
(7) Magnera, T. F.; David, D. E.; Stulik, D.; Orth, R. G.; Jonkman, H. T.; Michl, J. *J. Am. Chem. Soc.* **1989**, *111*, 5036.
(8) Magnera, T. F.; David, D. E.; Michl, J. *J. Am. Chem. Soc.* **1989**, *111*, 4100.
(9) Schultz, R. H.; Armentrout, P. B. *J. Phys. Chem.* **1993**, *97*, 596.
(10) Dalleska, N. F.; Honma, K.; Sunderlin, L. S.; Armentrout, P. B. *J. Am. Chem. Soc.* **1994**, *116*, 3519.
(11) Holland, P. M.; Castleman, A. W. *J. Am. Chem. Soc.* **1980**, *102*, 6174. Holland, P. M.; Castleman, A. W. *J. Chem. Phys.* **1982**, *76*, 4195.
(12) Dalleska, N. F.; Tjelta, B. L.; Armentrout, P. B. *J. Phys. Chem.* **1994**, *98*, 4191.
(13) Woodin, R. L.; Beauchamp, J. L. *J. Am. Chem. Soc.* **1978**, *100*, 501.
(14) Bojesen, G.; Breindahl, T.; Andersen, U. *Org. Mass Spectrom.* **1993**, *28*, 1448.
(15) Cerda, B. A.; Wesdemiotis, C. *J. Am. Chem. Soc.* **1996**, *118*, 11884.
(16) Clementi, E.; Popkie, H. *J. Chem. Phys.* **1972**, *57*, 1077.
(17) Kistenmacher, H.; Popkie, H.; Clementi, E. *J. Chem. Phys.* **1973**, *59*, 58842.
(18) Dierksen, G. H. F.; Kraemer, W. P. *Theor. Chim. Acta* **1975**, *36*, 249.
(19) Woodin, R. L.; Houle, F. A.; Goddard III, W. A. *Chem. Phys.* **1976**, *14*, 461.
(20) Del Bene, J. E.; Frisch, M. J.; Raghavachari, K.; Pople, J. A.; Schleyer, P. v. R. *J. Phys. Chem.* **1983**, *87*, 73.
(21) Del Bene, J. E.; Shavitt, I. *Int. J. Quantum Chem. Symp.* **1990**, *24*, 365.
(22) Kistenmacher, H.; Popkie, H.; Clementi, E. *J. Chem. Phys.* **1974**, *61*, 799.
(23) Feller, D.; Glendening, E. D.; Kendall, R. A.; Peterson, K. A. *J. Chem. Phys.* **1994**, *100*, 49881.
(24) Ervin, K. M.; Armentrout, P. B. *J. Chem. Phys.* **1985**, *83*, 166.
(25) Schultz, R. H.; Armentrout, P. B. *Int. J. Mass Spectrom. Ion Processes* **1991**, *107*, 29.
(26) Teloy, E.; Gerlich, D. *Chem. Phys.* **1974**, *4*, 417. Gerlich, D.; Diplomarbeit, University of Freiburg, Federal Republic of Germany, 1971. Gerlich, D. In *State-Selected and State-to-State Ion-Molecule Reaction Dynamics, Part I, Experiment*; Ng, C.-Y., Baer, M., Eds.; *Adv. Chem. Phys.* **1992**, *82*, 1.
(27) Aristov, N.; Armentrout, P. B. *J. Phys. Chem.* **1986**, *90*, 5135.
(28) Hales, D. A.; Armentrout, P. B. *J. Cluster Sci.* **1990**, *1*, 127.
(29) Schultz, R. H.; Crellin, K. C.; Armentrout, P. B. *J. Am. Chem. Soc.* **1992**, *113*, 8590.
(30) Dalleska, N. F.; Honma, K.; Armentrout, P. B. *J. Am. Chem. Soc.* **1993**, *115*, 12125.
(31) Schultz, R. H.; Armentrout, P. B. *J. Chem. Phys.* **1992**, *96*, 1046.
(32) Fisher, E. R.; Kickel, B. L.; Armentrout, P. B. *J. Phys. Chem.* **1993**, *97*, 10204.
(33) Fisher, E. R.; Kickel, B. L.; Armentrout, P. B. *J. Chem. Phys.* **1992**, *97*, 4859.
(34) Fogarasi, G.; Pulay, P. In *Vibrational Spectra and Structure*; Durig, J. R., Ed.; Elsevier: New York, 1985; Vol. 14, p 125.
(35) Beyer, T. S.; Swinehart, D. F. *Commun. ACM* **1973**, *16*, 379. Stein, S. E.; Rabinovitch, B. S. *J. Chem. Phys.* **1973**, *58*, 2438. Stein, S. E.; Rabinovitch, B. S. *Chem. Phys. Lett.* **1977**, *49*, 1883.
(36) Gilbert, R. G.; Smith, S. C. *Theory of Unimolecular and Recombination Reactions*; Blackwell Scientific Publications: Oxford, 1990.
(37) Loh, S. K.; Hales, D. A.; Lian, L.; Armentrout, P. B. *J. Chem. Phys.* **1989**, *90*, 5466.
(38) Waage, E. V.; Rabinovitch, B. S. *Chem. Rev.* **1970**, *70*, 377.
(39) Chesnavich, W. J.; Bowers, M. T. *J. Phys. Chem.* **1979**, *83*, 900.
(40) Armentrout, P. B. In *Advances in Gas Phase Ion Chemistry*; Adams, N. G., Babcock, L. M., Eds.; JAI: Greenwich, 1992; Vol. 1, pp 83−119.
(41) See, for example: Sunderlin, L. S.; Armentrout, P. B. *Int. J. Mass Spectrom. Ion Processes* **1989**, *94*, 149.
(42) See, for example, Figure 1 in: Dalleska, N. F.; Honma, K.; Armentrout, P. B. *J. Am. Chem. Soc.* **1993**, *115*, 12125.
(43) Armentrout, P. B.; Simons, J. *J. Am. Chem. Soc.* **1992**, *114*, 8627.
(44) Chase, M. W.; Davies, C. A.; Downey, J. R.; Frurip, D. J.; McDonald, R. A.; Syverupd, A. N. *J. Phys. Chem. Ref. Data* **1985**, *14* (Suppl. No. 1).
(45) Meyer, F.; Khan, F. A.; Armentrout, P. B. *J. Am. Chem. Soc.* **1995**, *117*, 9740.
(46) More, M. B.; Glendening, E. D.; Ray, D.; Feller, D.; Armentrout, P. B. *J. Phys. Chem.* **1996**, *100*, 1605. Ray, D.; Feller, D.; More, M. B.; Glendening, E. D.; Armentrout, P. B. *J. Phys. Chem.* **1996**, *100*, 16116.
(47) Weber, M. E.; Elkind, J. L.; Armentrout, P. B. *J. Chem. Phys.* **1986**, *84*, 1521.
(48) Lau, Y. K.; Ikuta, F.; Kebarle, P. *J. Am. Chem. Soc.* **1982**, *104*, 1462.
(49) Meot-Ner, M.; Speller, C. V. *J. Phys. Chem.* **1986**, *90*, 6616.
(50) Magnera, T. F.; David, D. E.; Michl, J. *Chem. Phys. Lett.* **1991**, *182*, 363.